

NOTICE CONCERNING COPYRIGHT RESTRICTIONS

This document may contain copyrighted materials. These materials have been made available for use in research, teaching, and private study, but may not be used for any commercial purpose. Users may not otherwise copy, reproduce, retransmit, distribute, publish, commercially exploit or otherwise transfer any material.

The copyright law of the United States (Title 17, United States Code) governs the making of photocopies or other reproductions of copyrighted material.

Under certain conditions specified in the law, libraries and archives are authorized to furnish a photocopy or other reproduction. One of these specific conditions is that the photocopy or reproduction is not to be "used for any purpose other than private study, scholarship, or research." If a user makes a request for, or later uses, a photocopy or reproduction for purposes in excess of "fair use," that user may be liable for copyright infringement.

This institution reserves the right to refuse to accept a copying order if, in its judgment, fulfillment of the order would involve violation of copyright law.

Improved Visualization of Satellite Radar InSAR Observed Structural Controls at Producing Geothermal Fields Using Modeled Horizontal Surface Displacements

Gary Oppliger¹, Mark Coolbaugh², and Lisa Shevenell³

¹Arthur Brant Laboratory for Exploration Geophysics, UNR

²Great Basin Center for Geothermal Energy, UNR

³Great Basin Center for Geothermal Energy, NBMG, UNR

Keywords

Reservoir structural controls, recharge, surface strain, InSAR, interferometry, radar, ground-water hydrology

ABSTRACT

Satellite radar InSAR observed deformation patterns around the Bradys, Nevada, USA producing geothermal system contain linear trends defined by steepened or inflected ground deformation gradients. We interpret these as structural controls on reservoir fluid flow (Oppliger et al., 2004 and 2005). We present results of a new technique to analyze these features using horizontal surface strains modeled from InSAR. Our methods allow quantitative mapping of horizontal strain on selected azimuths and the generation of the principal components from the horizontal strain tensor. Strains are mapped in qualitative units (e.g. parts-per-million) and characterized by their sign as tensile or compressive. We show that linear compressive surface strain patterns map directly above the flow axis of a contracting (i.e., cooling or de-pressurized) aquifer zone, whereas associated surface extension will lie outboard of the contracting zone. In the example case at Bradys, the contracting zone over the interferogram period is coincident with an approximately 14°C (25°F) drop in temperature and 14 kg/cm² (200 psi) drop in pressure (Holt et al., 2004).

Background

InSAR's ability to monitor surface deformation at geothermal fields has been well established on several fields (e.g., Coso: Fialko and Simons, 2000; Bradys: Oppliger, 2004) and models for inversion of reservoir volume-strain have been developed and applied (Vasco et al., 2002 and Oppliger et al., 2005).

Computing the 3-D Displacement Field

Our method utilizes a standard unwrapped InSAR LOS (line-of-sight) image selected for high signal-to-noise charac-

teristics. The general data preparation method is described in Oppliger et al. (2005). We apply elastostatic theory to find a Mogi (1958) source distribution that fits the observed LOS displacement and hence predicts the x, y and z components. A Mogi volume-strain source produces an isotropic (radial) displacement field; hence our solution assumes that no large fraction of the InSAR observed deformation field is contributed by fault plane dislocations, which are non-symmetric sources (Okada, 1985). We may deduce from the absence of a dipolar InSAR anomaly, inherent in strike-slip displacements,

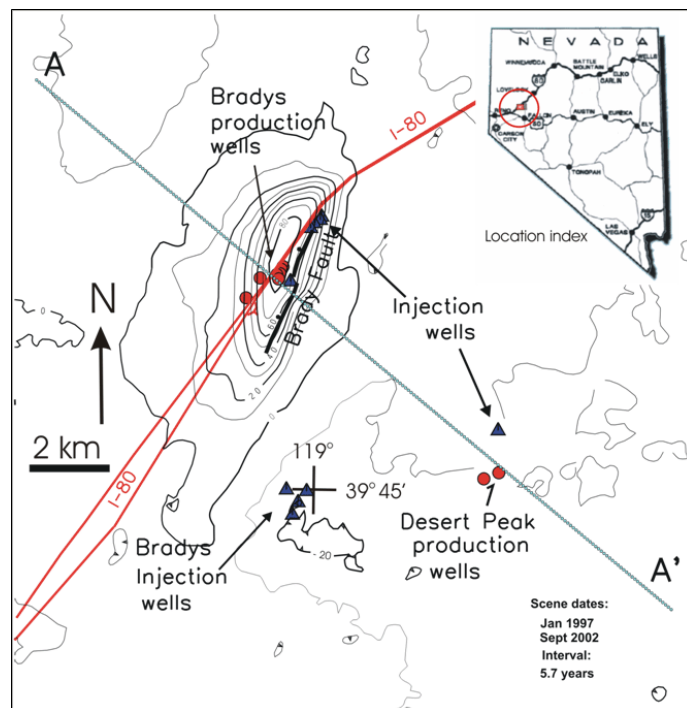


Figure 1. Plan map showing the Jan. 1997 to Sept. 2002 InSAR anomaly contoured at 10 mm intervals. The InSAR line-of-sight deformation has been modeled as vertical deformation in mm and filtered to remove signal from features with wavelengths less than 120 meters. Production and injection wells, Interstate Highway I-80, and model profile A-A' are shown for spatial reference. (Figure after Oppliger et al., 2005)

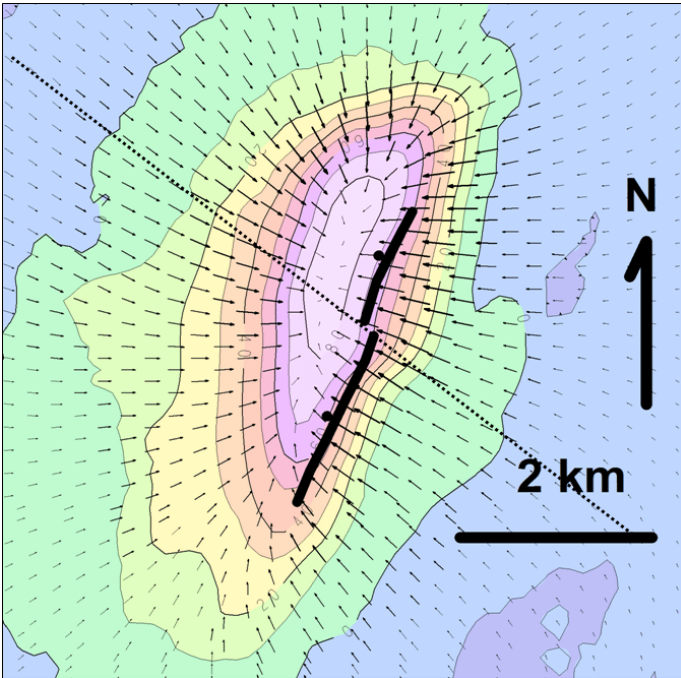


Figure 2. Plan view of the model-derived vertical and horizontal surface displacements for the 5.7 year observation period shown in Figure 1. Vertical displacement is contoured at 10 mm and horizontal displacement is represented by proportional length vectors that indicate a maximum displacement of about 65 mm. The dotted line crossing the NNW Brady fault (thick line with down side symbol) is the discussed analysis profile.

and the absence of fresh fault offsets that slip dislocations are not significant contributors to the InSAR observations. The full modeling technique is documented in a paper by Oppliger (in preparation).

In our example we describe the application of the technique to a 5.7 year InSAR displacement anomaly from the Brady Geothermal Field. (Figure 1). Figure 2 shows the vertical and horizontal displacement solutions for this observation period. Here, vertical displacement is contoured at 10 mm and horizontal displacement is represented by proportional length vectors which have a maximum displacement of ~65 mm. The dotted line crossing the NNW Brady fault is the analysis profile used in Figures 3 and 4. The horizontal surface displacement pattern clearly radiates toward the center of the produced geothermal field, which is dominantly localized along the west side of the surface expression of the Brady fault.

In Figure 3 we display the LOS, vertical and horizontal displacement patterns along the central segment of analysis profile AA'. By comparing the vertical displacement pattern to the original LOS displacement, it is seen that the vertical displacement peak is shifted relative to the LOS displacement by about 10% of the anomaly's wavelength in a direction away from the satellite radar illumination. Because it is free from horizontal displacement vector contributions, the vertical field provides a non-directionally biased view of the asymmetry induced by the reservoir's shape and attitude (dip) (Oppliger, 2005). We also note that the symmetry relation between vertical to horizontal displacement patterns show first order similar-

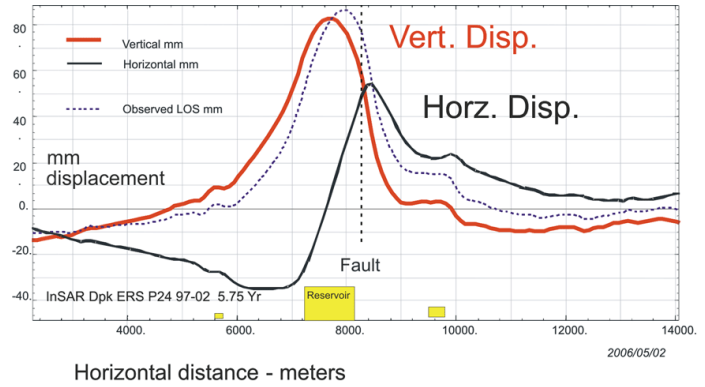


Figure 3. Section view of model derived vertical and horizontal surface displacements along a central segment of Brady profile AA'.

ity to that of a single Mogi volume strain source. The vertical displacement is nominally symmetric while the horizontal displacement is nominally anti-symmetric with the maximum horizontal displacement reaching about 50 percent of the maximum vertical displacement.

Horizontal Strains from the Displacement Field

Having estimated the horizontal displacement field, we proceed to find the horizontal surface strains. The horizontal displacement field is defined by a grid of displacement vectors (x_i, y_i) corresponding to the interferogram observation points, as represented by arrows in Figure 2. Surface strain information is contained in the spatial change rate or gradient of these displacement vectors and is completely expressed as a 2×2 tensor referred to as the displacement gradient tensor:

$$\nabla u = \begin{pmatrix} dx_i / dx & dx_i / dy \\ dy_i / dx & dy_i / dy \end{pmatrix}.$$

We map strains associated with structure around the geothermal field using two standard parameters from the displacement gradient tensor – firstly as directional strains along azimuths perpendicular to known geologic structure (Figure 4) and second as the principle strain components e_1 and e_2 or their sum, which is the total strain $e_1 + e_2$ (Figure 5). In both cases, the resulting strain values are expressed in quantitative ppm units and characterized by sign as tensional or compressive. Note ppm = parts-per-million; 1 ppm = 1 mm/km.

To find the directional strain we take the directional derivative of the displacement field in the selected direction. To find the principle strain components we compute the strain tensor E from the symmetric or non-rotational part of the displacement gradient tensor.

$$E = \begin{pmatrix} e_{xx} & e_{yx} \\ e_{xy} & e_{yy} \end{pmatrix} = \begin{pmatrix} dx_i / dx & (dy_i / dx + dx_i / dy) / 2 \\ (dy_i / dx + dx_i / dy) / 2 & dy_i / dy \end{pmatrix}$$

The strain tensor is then diagonalized so that its cross terms are zero and its e_{xx} and e_{yy} terms define the principal strains e_1 and e_2 of the associated strain ellipse.

$$E = \begin{pmatrix} e1 & 0 \\ 0 & e2 \end{pmatrix}$$

Total Strain = e1 + e2

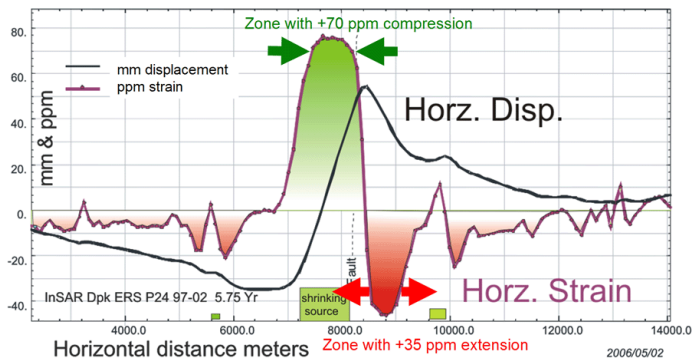


Figure 4. Modeled horizontal strain in ppm along the central segment of Bradys profile AA'.

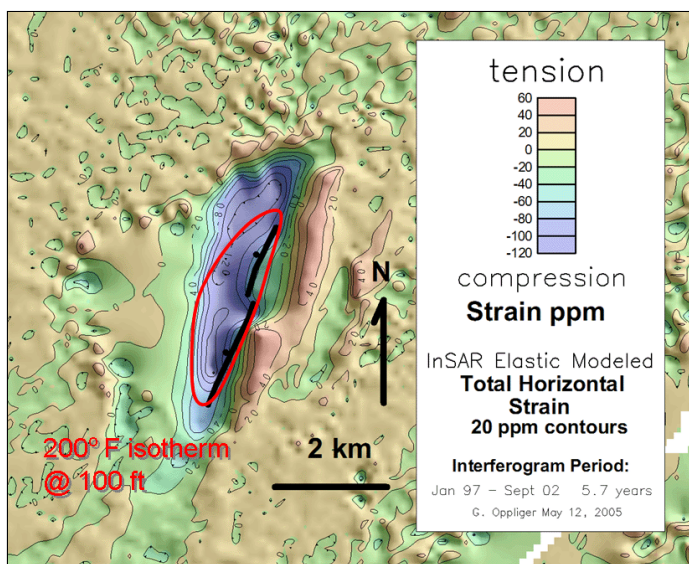


Figure 5. Map of modeled total horizontal strains (e1+e2) computed from strain analysis of the horizontal displacement field. The main compressive strain feature (in blue) west of the NNW Brady fault is interpreted as defining the reservoir's most significantly contracting zones; whereas, the main extensional area (orange color) to the east of the Brady fault is a result of peripheral elastic flexure in response to the reservoirs contraction. (Due to a difference in plot axis choice, the sign of the total horizontal strain is reversed compared to the profile in Figure 4.)

Model Results

Figures 4 and 5 show the maximum horizontal strain is compressive and localized directly over the reservoir (70 to 75 ppm over 5.7 years on the profile and ~120 ppm on the map). The maximum extensional strains are about half that magnitude and located peripheral to the reservoir's southeast

side (~35 ppm on the profile and ~50 ppm on the map). The northwestern dip of the Bradys reservoir system (which follows the NW-dipping Bradys fault system) accounts for the weaker extensional strain anomaly on the reservoir's northwest side. For a graphical representation of the northwesterly dipping reservoir and its relation to the InSAR anomaly see Oppliger et al., 2005.

To visually interpret the shape and location of a general sub-surface source, we use the following observational principles developed from forward modeling examples. We expect narrow width contracting source bodies will have local maximum compressive horizontal surface strains directly above their axes; while significantly wider, horizontal tabular contracting source bodies will show maximum compressive strains around the interior of their outer boundary trace. We also note that the local maximum extensional strain always develops exterior to a contracting body's surface trace due to elastic flexure. Where expanding sources are considered, the above horizontal compression and extension strain relations are interchanged.

Conclusions

The direct relation of compressive strain zones to contracting sources makes compressive strain zones a useful proxy to trace areas of reservoir cooling and pressure reduction.

Summary

We have developed a new technique to quantify gradients observed in InSAR LOS ground deformation patterns using horizontal surface strains modeled from InSAR. Our methods allow visualization of directional strain on selected azimuths and also as principal components of the horizontal strain tensor. Strains are mapped in qualitative units (e.g., ppm) and characterized by sign as tensional or compressive. We show that local maximum compressive surface strain patterns are expected to map directly above the flow axis of a contracting (cooling or de-pressurized) aquifer structure, whereas local maximum extension strains will lie outboard of the contracting zone. The mapped contracting zone over the interferogram period is coincident with approximately 14°C (25°F) and 14 kg/cm² (200 psi) drops in temperature and pressure (Holt et al., 2004).

Acknowledgements

This material is based upon work supported in part by the Department of Energy, Golden Field Office, under Award Number DE_FG36-02ID14311. Additional support was provided by the Arthur Brant Laboratory for Exploration Geophysics, University of Nevada Reno. JPL ROI_PAC v2.2.2 Repeat Orbit Interferometry radar processing software was utilized. Some of the raw ERS 1 & 2 radar scenes were provided by the WInSAR Consortium. Precise Orbits for the ERS 1 & 2 satellites were obtained from Delft Institute, The Netherlands.

Disclaimer

This report was prepared as an account of work sponsored by an agency of the United States Government. Neither the United States Government nor any agency thereof, nor any of their employees, makes any warranty, express or implied, or assumes any legal liability or responsibility for the accuracy, completeness, or usefulness of any information, apparatus, product, or process disclosed, or represents that its use would not infringe privately owned rights. Reference herein to any specific commercial product, process or service by trade name, trademark, manufacturer, or otherwise does not necessarily constitute or imply its endorsement, recommendation, or favoring by the United States Government or any agency thereof. The views and opinions or authors expressed herein do not necessarily state or reflect those of the United States Government or any agency thereof.

References

Fialko, Y., and M. Simons, 2000, Deformation and seismicity in the Coso geothermal area, Inyo County, California: Observations and modeling using satellite radar interferometry, *Journal of Geophysical Research*, v. 105, p. 21,781-21,794.

Holt, R., D. Campbell, and S. Matlick, 2004, Reservoir simulation of Bradys geothermal field, Nevada. *Geothermal Resources Council Transactions*, v. 28, p. 589-593.

Mogi, K., 1958, Relations between the eruptions of various volcanoes and the deformations of the ground surface around them, *Bull. Earthquake Res. Inst. Univ. Tokyo*, v. 36, p. 99-134.

Okada, Y., 1985, Surface deformation due to shear and tensile faults in a half-space, *Bull. Seis. Soc. Am.*, v. 75, 1135-1154.

Oppliger, G., Coolbaugh, M. Foxall, W., 2004, Imaging Structure with Fluid Fluxes at the Bradys Geothermal Field with Satellite Interferometric Radar (InSAR): New Insights into Reservoir Extent and Structural Controls, v. 28, p. 27-40.

Oppliger, G., M.F. Coolbaugh, L. Shevenell, and J.V. Taranik. 2005. Elucidating deep reservoir geometry and lateral outflow through 3-D elastostatic modeling of satellite radar (InSAR) observed surface deformations, *Geothermal Resources Council Transactions*, v. 29: 419-424.

Oppliger, G., in prep, Modeling full 3-D displacement fields directly from differential InSAR observations.

Vasco D.W., Wicks, C., Jr., and Karasaki, K., 2002, Geodetic imaging: High-resolution reservoir monitoring using satellite interferometry, *Geophysical Journal International*, v. 149, p. 555-571.